OPEN ACCESS

University of Dundee

University of Dundee

Physical modelling of soil-structure interaction of tree root systems under lateral loads

Zhang, Xingyu; Knappett, Jonathan; Leung, Anthony; Liang, Teng

Published in:
Physical Modelling in Geotechnics

DOI:
10.1201/9780429438646

Publication date:
2018

Document Version
Peer reviewed version

Link to publication in Discovery Research Portal

Citation for published version (APA):
Zhang, X., Knappett, J., Leung, A., & Liang, T. (2018). Physical modelling of soil-structure interaction of tree root systems under lateral loads. In A. McNamara, S. Divall, & R. Goodey (Eds.), *Physical Modelling in Geotechnics: Proceedings of the 9th International Conference on Physical Modelling in Geotechnics (ICPMG 2018), July 17-20, 2018, London, United Kingdom* (Vol. 1, pp. 481-486). Taylor & Francis.
https://doi.org/10.1201/9780429438646

General rights
Copyright and moral rights for the publications made accessible in Discovery Research Portal are retained by the authors and/or other copyright owners and it is a condition of accessing publications that users recognise and abide by the legal requirements associated with these rights.

Take down policy
If you believe that this document breaches copyright please contact us providing details, and we will remove access to the work immediately and investigate your claim.

Download date: 09. Oct. 2025

Author Accepted Manuscript version of Zhang, X, Knappett, J, Leung, A & Liang, T 2018, Physical modelling of soil-structure interaction of tree root systems under lateral loads. in A McNamara, S Divall & R Goodey (eds), Physical Modelling in Geotechnics: Proceedings of the 9th International Conference on Physical Modelling in Geotechnics (ICPMG 2018), July 17-20, 2018, London, United Kingdom. vol. 1, Taylor & Francis, pp. 481-486, 9th International Conference on Physical Modelling in Geoetchnics, London, United Kingdom, 17/07/18. https://doi.org/10.1201/9780429438646

Physical modelling of soil-structure interaction of tree root systems under lateral loads

Zhang, X., Knappett, J.A., Leung, A.K., & Liang, T.
University of Dundee, UK

ABSTRACT: This paper presents some initial physical modelling of root-soil interaction for trees under lateral loading, such as from wind or debris flows. 3-D printing of interconnected systems of ABS plastic root analogues, which are mechanically representative of tree roots, is used to produce idealised root architectures with varying root depth, spread and root area ratio (*RAR*, i.e. amount of roots). These models are installed within a granular soil with a wooden model trunk attached and laterally loaded to measure the push-over behaviour. From this data, the moment capacity and rotational stiffness of the model root systems are evaluated. The results suggest that (i) the effect of the central tap root on strength and stiffness is low, compared to the lateral and sinker roots, but otherwise proportional to RAR; and (ii) that development of analytical predictive models may be able to adapt existing procedures for conventional geotechnical systems, such as pile groups.

1 INTRODUCTION

1.1 *Background*

Understanding 'windthrow' of trees (their behaviour under strong lateral wind loads) has long been of interest in forestry, where it is important for understanding how much of a crop may be damaged by bad weather and how selective planting may be used to protect stands of vulnerable trees (Ulanova, 2000; Gardiner & Quine, 2000; Mickovski et al., 2005). It is also of interest in civil engineering, where windthrow of trees on sloping ground may be a trigger for landsliding, or where fallen trees may disrupt transportation services, such as occurred in the UK during Storm Doris in February 2017, where a fallen tree brought down overhead power lines on the West Coast Mainline. While research has previously been conducted into the subaerial aspects of this problem (i.e. fluid-structure interaction, e.g. Langre, 2008), little is known about how to model the interaction between the tree and the ground through the root system, which acts as a foundation of highly complex geometry. This is important as changing ground conditions (e.g. due to rainfall accompanying high winds) may soften and weaken the ground and increase the vulnerability of a tree to overturning.

1.2 *Aims and objectives*

In this paper, two contrasting 1:10 scale root systems were designed. One type is narrow and deep while the other is wide and shallow. Different numbers, sizes and distributions of roots were also considered to construct root system with different root area ratio (*RAR*). 3-D printing techniques were employed to fabricate these models using Acrylonitrile Butadiene Styrene (*ABS*) plastic material, which has mechanical properties highly similar to tree roots and has been used by other researchers to create root models for studying slope stabilisation by vegetation (e.g. Liang et al., 2015; Meijer et al., 2016; Liang & Knappett, 2017). The models were subsequently embedded into soil with model tree trunks connected to the top. A linear actuator was then used to conduct lateral load tests close to the bottom of the trunk to measure the rotational stiffness and moment capacity of the root systems acting as foundations, and including the second-order P-Δ effects from the trunk.

2 ROOT MODELLING

2.1 *Trunk, stump and rooted zone geometry*

Root area ratio (*RAR*) is an important characteristic when describing a root system. It refers to the proportion of total root cross sectional area within the zone of rapid taper (*ZRT*), a zone that includes most of structural roots with a radius conventionally defined as approximately 2.17 times bigger than the diameter at breast height (*DBH*; Danjon et al., 2005). In order to quantify the influence of *RAR*, three *RAR*s are considered here, namely 0.5%, 2.0% and

4.5%, and this is believed to cover a wide range of species (Mao et al., 2012).

The thick main stem of a tree, which is also called the trunk, transfers lateral loading directly to the root system via the stump. According to research conducted by Danjon et al., (2008), the diameter of the stump has been observed in the field to be approximately 250 mm for some tree species in slopes. This value was adopted in this study, resulting in a stump 25 mm in diameter at 1:10 scale. To simplify the design of the tree model and subsequent analysis, a circular trunk was designed having the same diameter, constant with height, such that *DBH* was 25 mm. The length of the trunk was 750 mm, thereby representing a tree 7.5 m tall.

For the selected *DBH*, the *ZRT* dimensions of the short and wide root system would exceed the threshold of the available 3-D printer. In order to make the models printable, the *ZRT* was set to twice the *DBH*, for both the deep and shallow model systems.

2.2 *Root system*

Liang et al. (2015, 2017) reported a prototype tree root system that was constructed based on the statistical data of tree root characteristics available in the literature. The system was shown to provide similar direct shear behavior to real root systems. This study bases on the same prototype root system to develop model root analogues for studying active push-over loading. The analogues were made of vertical circular rods of constant diameter (i.e. no tapering with distance from the stump). Five distinct types of root analogues with diameter 12 mm (just for the tap root below the stump), 5 mm, 3 mm, 1.6 mm and 0.8 mm were used within the design of the model root systems in this paper, which is consistent with previous work (Liang et al., 2015; 2017). The root architecture was idealized as a perforated circular disc at the ground surface, consisting of lateral 'spokes' and circumferential rings, mechanically connecting the set of vertical root analogues to the stump.

A range of *RAR* values between 0.5% and 4.5% was selected. It should be noted that for *RAR* = 0.5%, the central tap root (immediately beneath the stump) was not included because in this case, the overall total root cross sectional area was smaller than the cross sectional area of a single tap root. Finally, three values of *RAR* (0.57%, 2.01% and 4.47%) were selected to use. It should be noted that the only difference between the models of *RAR* = 0.5% and *RAR* = 2.0% was only the addition of a single tap root at the centre of the root system. The number of each size of root analogue in each model system is shown in Table 1.

Table 1. Root numbers for the deep and narrow root system

RAR	Diameter of individual root: mm				
	12 (tap)	5	3	1.6	0.8
0.57%	0	1	2	4	6
2.01%	1	1	2	4	6
4.47%	1	4	13	25	34

The cumulative root fraction (percentage of the total amount of roots within a certain distance from the stump) decreases sharply with increasing depth below the ground surface and for trees, shrubs and grasses, at least 90% of the cumulative root fraction reaches to 1 m depth (Jackson et al., 1996). So the deepest and narrowest model root system was designed to be 100 mm deep at model scale. The shallower, wider root system represents the case of the roots being half as deep, but with twice the plan area, without changing the *RAR* (i.e. having twice the number of each size of root analogue from Table 1, each being half the length).

The computer-aided design software Solidworks was used to construct the root system models and generate an input file for the 3-D printer. The vertical root analogues were distributed across five concentric rings forming the surface disc. The thickness of the rings and of the spokes connecting them was 3 mm, which was consistent with Sonnenberg et al., (2010) and the width of rings were designed to also be 3 mm. The spokes represent stiff lateral branches off the main tap root (see Fig. 1). The width of the eight uniformly distributed spokes ranges from 0 mm at the central point to 6 mm at edge, such that the average width was also 3 mm.

In this study, individual roots and perforated discs were printed separately, with the discs incorporating printed holes, 2 mm in depth, for subsequent attachment of the root analogues. In addition, a coupler with 25 mm internal diameter, 10 mm in height and 1 mm in thickness was designed to attach the trunk to the stump.

2.3 *Model fabrication and assembly*

The model roots were fabricated from Acrylonitrile Butadiene Styrene (*ABS*) plastic which was chosen as its properties are similar to those of real roots (Liang et al., 2015; 2017). All of the models were fabricated using a Stratesys Inc. uPrint SE *ABS* rapid prototyper (3-D printer) at the University of Dundee. The fabrication process, which involves progressive layering of the ABS plastic was exploited to print the root analogues with the layering running along the vertical root axis, to approximate the fibrous structure of real roots (Liang et al., 2014).

Epoxy resin adhesive was used to connect the root analogues with the disc. This required some abrasion of the printed holes to ensure the root ana-

logues would fit snugly. Some assembled model root systems are shown in Figure 2.

3 TEST METHODOLOGY

A 900 mm × 450 mm × 450 mm box, which is large enough to avoid boundary effects, was used to contain HST95 Congleton silica sand. This material was pluviated in air to a relative density of approximately 50% for each test. Root system models were subsequently pushed into the soil after pluviation, this being similar to root growth in reality.

Lateral force was applied using a GDS Force Actuator (GDSFA), which is a general purpose electrically driven uniaxial loading system with feedback control and continuous displays of force and displacement. This paper reports only push-over tests to large displacement (90 mm), which were conducted under displacement control at a constant speed of 6 mm/min. Force and displacement readings were logged at a sampling frequency of 1 Hz.

The loading was applied towards the bottom of trunk, 140 mm above the ground surface. A trolley was used to raise the model container to this height. The wheels of the trolley were locked during testing to ensure there was no displacement of the reference frame. The geometry of the test setup is shown in Figure 3. The thickness of box base was 30 mm and the soil 350 mm in depth.

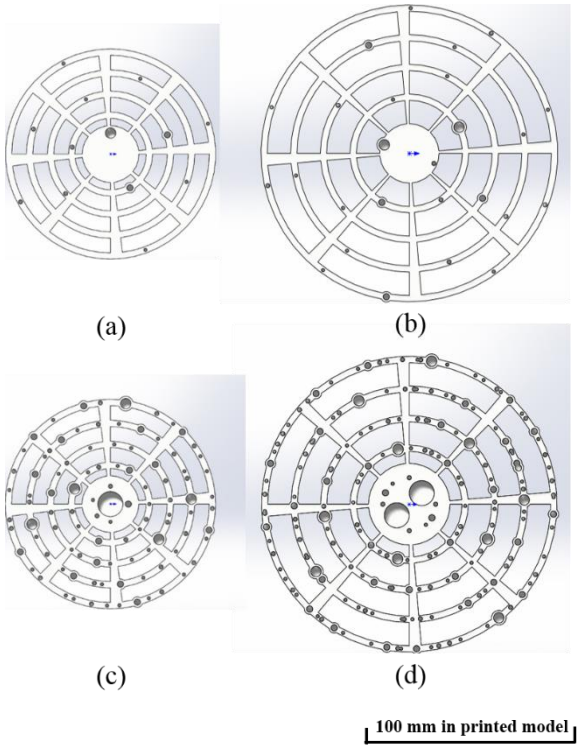

Figure 1. Root system constructed in Solidworks: (a) & (c) represent a deep and narrow root system with *RAR* = 0.57% and 4.47% respectively; (b) & (d) represent a shallow and wide root system with *RAR* = 0.57% and 4.47% respectively

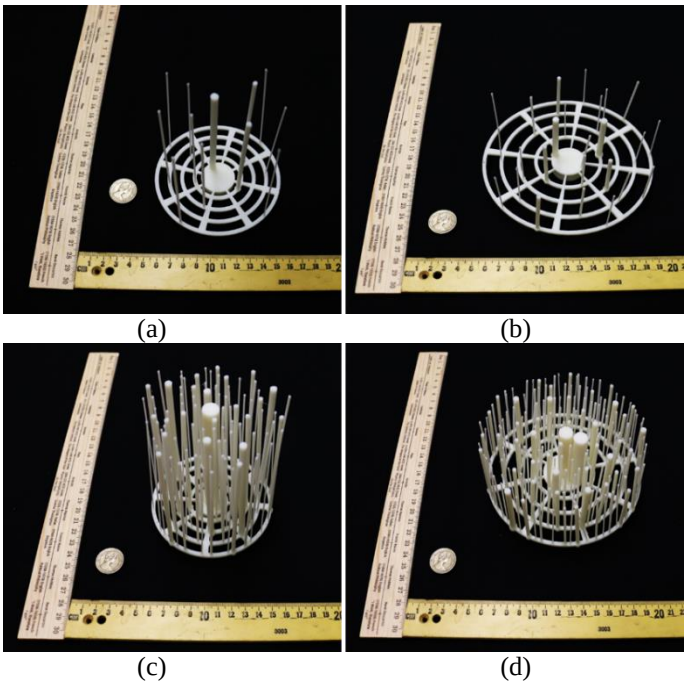

Figure 2. 3-D printed root system model: (a) & (c) show the deep and narrow root system with *RAR* = 0.57% and 4.47% respectively; (b) & (d) show the shallow and wide root system with *RAR* = 0.57% and 4.47% respectively

4 RESULTS AND DISCUSSION

4.1 *Push-over curves*

Figure 4 shows the direct results of pushover curves measured for the different types of root system. It can be seen that, in general, the push-over force experienced a rapid increase in the initial stage of the test. However, after reaching a certain value, the push-over force decreases at a similar rate with initial increase. For the deep and narrow root system, the behavior differs between smaller and larger displacements, the reason for which will be discussed later. The push-over curves exhibit some noise. A possible reason is that when roots are pushed to move, no matter horizontally or vertically, root-soil interface friction generated may not be uniform in dry sand because of the shape of the sand particles in contact with the roots However, further experiments are needed to confirm this.

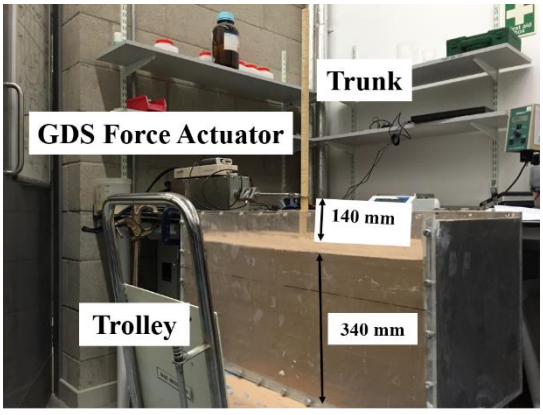

Figure 3. Schematic test setup

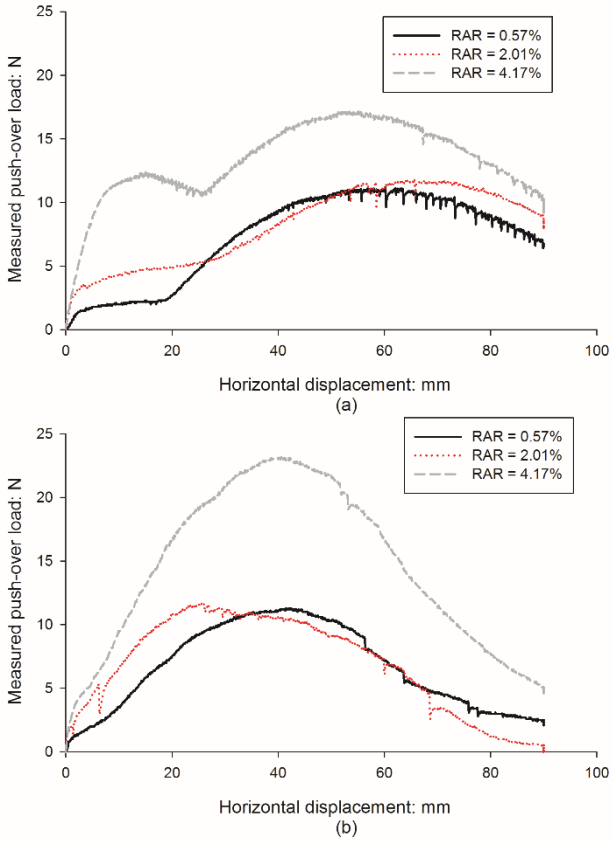

Figure 4. Push-over curve for (a) deep and narrow root system and (b) shallow and wide root system, with different values of *RAR*

4.2 *Root system moment capacity*

The variation of moment capacity with *RAR* is shown in Figure 5. It can be seen that in general, moment capacity grows with the increase of *RAR* from 2.01% to 4.47%, while no obvious difference can be observed when *RAR* changes from 0.57% to 2.01%. It is important to state at this stage that the only difference between the root systems with *RAR* = 0.57% and *RAR* = 2.01% is the presence of the central tap root (two central adjacent tap roots in the case of the shallow and wide root system). In this case, it is reasonable to say that the tap root(s) makes few contributions to the moment capacity, while the smaller diameter roots spaced further away from the trunk have a more significant effect on the moment capacity of the root system.

It is also evident from Figure 5 that the shallow and wide root system, which has the same amount of root material and the same surface area of the root analogues, has a much larger resistance to overturning at higher *RAR*. This is consistent with the moment capacity being the sum of the individual root pull-out capacities in each case multiplied by the radius from the trunk. At lower *RAR* (< 2%) this effect is not apparent, possibly because the increased moment capacity due to the increased radius is offset by the lower average effective confining stress along

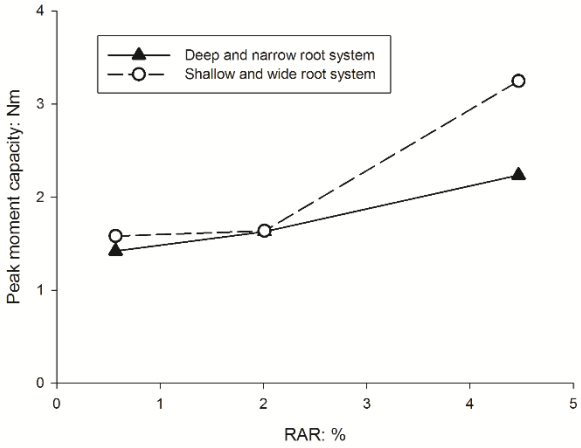

Figure 5. Moment capacity for different types of root systems with different root area ratio

the analogues, given their reduced length and the low number of roots in these models.

In the case of *RAR* = 4.47%, the more than doubling in root material from the *RAR* = 2.01% case, offsets the reduction (by approximately half) in the confining stress on its own, explaining the increased effectiveness of this case. This is not true in increasing *RAR* to 2.01% from the 0.57% case, as all of the increase is concentrated in the large tap roots, the pull-out resistances of which are not mobilised fully due to their position immediately beneath the trunk.

4.3 *Failure mechanism*

Two types of failure modes were observed in the tests presented here: (i) overturning of the whole system involving extensive pull-out of the vertical root analogues on the 'windward' side (Fig.6(a)); and (ii) breakage of the lateral branches close to the trunk (Fig. 6(b)). These two failure mechanisms could occur either separately or simultaneously.

For shallow and wide root systems, as the horizontal displacement increased, the lateral branches on the 'leeward' side broke, with sinker roots on windward side only partially pulled out from the soil (i.e. mechanism (ii); Fig. 6(b)).

For deep and narrow root systems, both mechanisms occurred during the tests, resulting in the distinctive flattening or drop in the push-over curve at smaller displacement (Fig. 4(a)). The whole system therefore overturns (i.e., root pull-out; mechanism (i), Fig. 6(a)) at lower displacement, and exhibits the first peak resistance shown in Fig. 4(a) (i.e., around 2 N, 4 N and 12 N for increasing *RAR*). As the horizontal displacement increases further, the resistance provided by the lateral branches is increasingly mobilised, causing the second higher peak in Fig. 4(a). The subsequent drop of push-over load is because of the breakage of the lateral branches (mechanism (ii); Fig. 6(b), similar to what is observed in the shallow and wide root system.

For all tests, no single vertical root was broken during the pushover process. In other words, lateral roots are more vulnerable to be damaged during push-over compared to sinker roots.

4.4 *Root system stiffness*

The following equation was used to calculate the total stiffness of root system, to account for the flexibility in the 140 mm of trunk between the load point and the soil surface:

$$K_{total} = \frac{1}{h^2\left(\frac{h}{3EI} + \frac{1}{K_r}\right)} \quad (1)$$

where h refers to the distance between loading point and bottom of trunk, E is the flexural modulus of trunk, I is for second moment of area of trunk and K_r is the rotational stiffness of the root system. This equation is derived from considering the lateral force-displacement behavior of a linear elastic cantilever with a rotational spring at the point of fixity.

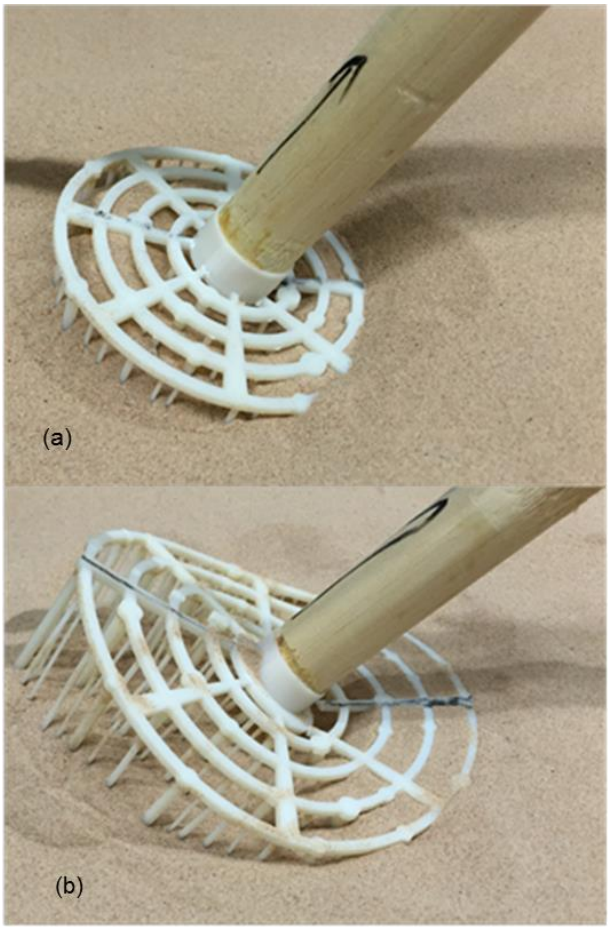

Figure 6. Different failure mechanisms observed in the tests (a): overturning of the whole root system; (b) breakage of the lateral branches close to trunk

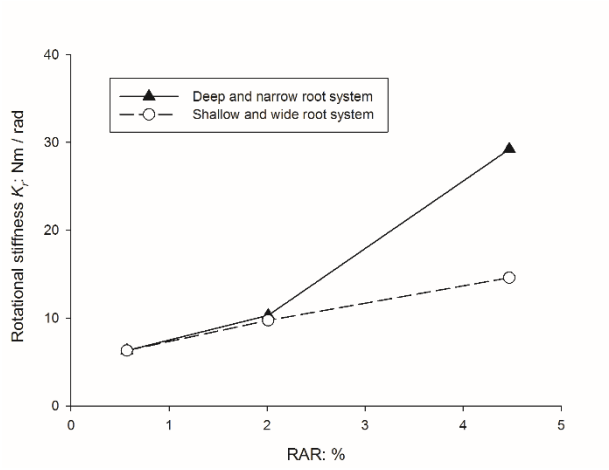

Figure 7. Rotational stiffness for different root systems with different root area ratio

The properties of the trunk were obtained from conducting four-point bending tests on n = 6 samples. The mean value of E was 0.502 MPa, the coefficient of variation was 11.8% and the mean value of EI was therefore 86.188 Nm^2.

Using Equation (1) it was found that the displacement caused by trunk bending was 10^3 times smaller than that triggered by rotation and could be ignored. As a result, $K_{total} \approx K_r$ and was determined by linear fitting of the lateral moment-rotation curves, up to moments half of the maximum moment capacity. The value of K_r for each case is shown in Figure 7. It can be seen that the rotational stiffness of deep and narrow root system is larger than that of shallow and wide one, which is contrary to the observation made earlier for moment capacity. This is because up to half of the maximum moment capacity, the lateral roots have not broken in either test - if these control the initial lateral stiffness, then the reduced length of these roots in the deep and narrow case provides greater stiffness against bending.

Figure 7 also suggests that the lateral surface roots make a larger contribution to rotational stiffness than the tap root.

5 CONCLUSIONS

All of the factors considered (e.g. root type and root area ratio) in this study were observed to influence the stiffness and capacity of tree root systems in soil under lateral loadings. Deep and narrow root systems show higher rotational stiffness at larger *RAR* while shallow and wide root systems show larger moment capacity. So when using trees to mitigate against different types of hazards, different species should be considered, depending on whether the design requires that the trees should remain stable (e.g. trees on sloping ground or next to transport infrastructure) or whether they are sacrificial (e.g. as exterior protection for large stands of commercial forest).

It has also been shown that stiffness is largely controlled by the near-surface lateral roots bending, while moment capacity is controlled by pull-out of vertical sinker roots. This suggests that existing analytical models for foundations (e.g. soil-structure interaction for flexible rafts/beams or overturning resistance of large pile groups) may be adapted for analysing tree root systems under lateral loading.

6 REFERENCES

Danjon F, Fourcaud T and Bert D, 2005. Root architecture and wind-firmness of mature Pinus pinaster. New Phytologist 168(2): 387–400.

Danjon F, Barker DH, Drexhage M and Stokes A, 2008. Using three-dimensional plant root architecture in models of shallow-slope stability. Annals of Botany 101(8): 1281–1293.

Gardiner BA and Quine CP, 2000. Management of forests to reduce the risk of abiotic damage - a review with particular reference to the effects of strong winds. Forest Ecology and Management 135: 261–277.

Jackson RB, Canadell J, Ehleringer JR, et al., 1996. A global analysis of root distributions for terrestrial biomes. Oecologia 108(3): 389–411.

Langre E De , 2008. Effects of Wind on Plants. Annual Review of Fluid Mechanics 40: 141–168.

Liang T, Knappett JA and Bengough AG, 2014. Scale modelling of plant root systems using 3-D printing. In *ICPMG2014–Physical Modelling in Geotechnics, Perth, Australia, 14-17 January 2014. pp: 361–366.*

Liang T, Knappett JA and Duckett N, 2015. Modelling the seismic performance of rooted slopes from individual root–soil interaction to global slope behaviour. Géotechnique 65(12): 995–1009.

Liang T and Knappett JA, 2017. Centrifuge modelling of the influence of slope height on the seismic performance of rooted slopes. Géotechnique 67(10): 855–869.

Liang T, Knappett JA, Bengough AG and Ke YX, 2017. Small scale modelling of plant root systems using 3-D printing , with applications to investigate the role of vegetation on earthquake induced landslides. Landslides 14(5): 1747–1765.

Meijer GJ, Bengough AG, Knappett JA, et al., 2016. New in situ techniques for measuring the properties of root-reinforced soil – laboratory evaluation. Géotechnique 66(1): 27–40.

Mickovski SB, Stokes A and Beek LPH Van, 2005. A decision support tool for windthrow hazard assessment and prevention. Forest Ecology and Management 216: 64–76.

Sonnenberg R, Bransby MF, Bengough AG, et al., 2011. Centrifuge modelling of soil slopes containing model plant roots. Canadian Geotechnical Journal 49(1): 1–17.

Ulanova NG , 2000. The effects of windthrow on forests at different spatial scales : a review. Forest Ecology and Management 135: 155–167.